

## A cell-free DNA metagenomic sequencing assay that integrates the damage response to infection

**Authors:** Alexandre Pellan Cheng<sup>1</sup>, Philip Burnham<sup>1</sup>, John Richard Lee<sup>2,3</sup>, Matthew Pellan Cheng<sup>4,5</sup>, Manikkam Suthanthiran<sup>2,3</sup>, Darshana Dadhania<sup>2,3,\*</sup>, Iwijn De Vlaminck<sup>1,\*</sup>

\*Correspondence should be addressed to D.D. ([dmd2001@med.cornell.edu](mailto:dmd2001@med.cornell.edu)) or to I.D.V. ([vlaminck@cornell.edu](mailto:vlaminck@cornell.edu)).

\*These authors contributed equally to this work.

### **Affiliations:**

<sup>1</sup> Meinig School of Biomedical Engineering, Cornell University, Ithaca, NY 14853, USA

<sup>2</sup> Division of Nephrology and Hypertensions, Department of Medicine, Weill Cornell Medicine, New York, NY 10065, USA

<sup>3</sup> Department of Transplantation Medicine, NewYork-Presbyterian Hospital-Weill Cornell Medical Center, New York, 10065, USA

<sup>4</sup> Division of Infectious Diseases, Brigham and Women's Hospital, Boston, MA 02115, USA

<sup>5</sup> Department of Medical Oncology, Dana-Farber Cancer Institute, Boston, MA 02115, USA

### **ABSTRACT**

High-throughput metagenomic sequencing offers an unbiased approach to identify pathogens in clinical samples. Conventional metagenomic sequencing however does not integrate information about the host, which is often critical to distinguish infection from infectious disease, and to assess the severity of disease. Here, we explore the utility of high-throughput sequencing of cell-free DNA after bisulfite conversion to map the tissue and cell types of origin of host-derived cell-free DNA, and to profile the bacterial and viral metagenome. We applied this assay to 51 urinary cfDNA isolates collected from a cohort of kidney transplant recipients with and without bacterial and viral infection of the urinary tract. We find that the cell and tissue types of origin of urinary cell-free DNA can be derived from its genome-wide profile of methylation marks, and strongly depend on infection status. We find evidence of kidney and bladder tissue damage due to viral and bacterial infection, respectively, and of the recruitment of neutrophils to the urinary tract during infection. Through direct comparison to conventional metagenomic sequencing as well as clinical tests of infection, we find this assay accurately captures the bacterial and viral composition of the sample. The assay presented here is straightforward to implement, offers a systems view into bacterial and viral infections of the urinary tract, and can find future use as a tool for the differential diagnosis of infections.

## 1 INTRODUCTION

2  
3 Differential diagnosis of infectious disease in humans is complex. Metagenomic high-throughput  
4 DNA sequencing offers an unbiased approach for the detection of pathogens in clinical samples<sup>1-</sup>  
5 <sup>4</sup>, but the presence of a pathogen is not necessarily synonymous with disease<sup>5</sup>. Some microbes  
6 are commensals in all human hosts, some only cause disease in some hosts, and others cause  
7 disease in all hosts. To bring clarity to the lexicon of microbial pathogenesis, Casadevall and  
8 Pirofski defined infectious disease as a clinical manifestation of damage to the host that results  
9 from host-microbe interaction<sup>5,6</sup>. In this framework, the degree of host damage, mediated by the  
10 host response and/or by the pathogen, offers a quantifiable metric that can be used to distinguish  
11 between different outcomes of infection<sup>6</sup>.

12  
13 We report a high-throughput metagenomic sequencing assay that can both detect a diverse array  
14 of bacterial and viral pathogens and quantify damage to host tissues. The assay implements  
15 whole-genome bisulfite sequencing (WGBS) of cell-free DNA (cfDNA), small fragments of DNA  
16 released by host or microbial cells into blood, urine and other bodily fluids, and brings together  
17 two previously reported concepts. First, the assay implements a genome-wide measurement of  
18 cytosine methylation marks comprised within cfDNA – marks that are highly cell, tissue and organ-  
19 type specific – to determine the cell and tissue types that contribute to the mixture of host cfDNA  
20 in a sample. Several recent studies have shown that profiling CpG methylation marks in urinary  
21 or plasma cfDNA, via whole-genome sequencing, targeted sequencing, or PCR assays, can be  
22 used to determine their tissues-of-origin and to quantify tissue-specific injury in various diseased  
23 settings<sup>7-9</sup>. Here, we explore this concept for the monitoring of injury due to infection. Second,  
24 the assay quantifies the relative abundance of microbes via WGBS of cfDNA. Several studies  
25 have investigated the utility of conventional, metagenomic sequencing of cfDNA for infection  
26 testing in clinical samples<sup>2,4,10,11</sup>. We show here that WGBS is compatible with such analyses.

27  
28 We investigated the utility of this assay to monitor infectious complications of the urinary tract  
29 after kidney transplantation. More than 80,000 patients receive lifesaving kidney transplants  
30 worldwide each year<sup>12</sup>. Immunosuppression after transplantation is required to manage the risk  
31 of rejection but leaves patients vulnerable to viral and bacterial infection. BK Polyomavirus (BKV)  
32 infection has emerged as serious risk factor for allograft survival. BKV reactivation occurs in up  
33 to 73% of kidney transplant recipients, and leads to BK Polyomavirus Nephropathy (BKVN) in up  
34 to 8% of patients<sup>13,14</sup>. Renal biopsies are currently required to confirm BKVN and to distinguish  
35 BKVN from BKV reactivation without nephropathy (BKV+/N-). While BKVN histology is  
36 characterized by inflammation and necrosis of tissue, biopsies from BKV+/N- patients are similar  
37 to those without reactivation<sup>13</sup>. It remains unclear whether BKV reactivation alone induces kidney  
38 damage. Bacterial urinary tract infection (UTI) affects approximately 43% of kidney transplant  
39 recipients in the first 42 months post-transplant<sup>15</sup>. There is a disagreement in the literature  
40 regarding the appropriate balance between mitigating the risks of infectious complications and  
41 adverse effects of antimicrobial treatment for UTI. In this study, we describe a urinary cfDNA  
42 assay that can identify viral and bacterial infectious agents and can quantify the degree of host  
43 injury related to UTI.

44

## 1 RESULTS

2

### 3 Methylation marks are cell, tissue and organ type specific

4

5 We performed WGBS (**Fig. 1a**) on 51 urinary cfDNA isolates collected from a cohort of kidney  
6 transplant recipients (**Fig.1b**) and used computational methods to quantify the burden of viral and  
7 bacterial cfDNA and the cell and tissue types of origin of host-derived cfDNA (**Fig.1c**). We  
8 assayed urinary cfDNA isolates from patients who had a same-day corresponding bacterial  
9 culture (UTI positive, UTI group, n=12; UTI negative, no-UTI group, n=12), and from patients that  
10 were BKV positive in the blood and confirmed to have BKVN by biopsy (BKVN, n=9), BKV positive  
11 in the blood without evidence of BKVN on biopsy (BKVN+/N-, n=7) and negative for BKV in the  
12 blood and with normal surveillance biopsy (Normal, n=6). In addition, we analyzed urinary cfDNA  
13 obtained from patients within the first three days after transplantation (Early group, n=5). To obtain  
14 sequence information after bisulfite conversion of these molecules, we used a single-stranded  
15 sequencing library preparation<sup>1,16</sup> (**Fig. 1a**). This library preparation employs ssDNA adapters and  
16 bead ligation to create diverse sequencing libraries from short, highly fragmented cfDNA<sup>16,17</sup>. We  
17 obtained 104.5 +/- 43 million paired-end reads per sample, corresponding to a per-base human  
18 genome coverage of 1.4-4.1x (see Methods).

19

20 We sought to implement a reference-based approach for cell-type deconvolution, thereby taking  
21 advantage of the large and growing number of genome-wide methylation profiles of tissues and  
22 cell types of interest that are available in public repositories. We downloaded 112 genome-wide  
23 methylation datasets representing 16 different tissue types (**Supplemental table 1**)<sup>18-22</sup>, and  
24 determined tissue-specific differentially methylated regions (DMRs) using Metilene<sup>23</sup>. We  
25 compared CpG methylation profiles of each tissue group in a one-versus-one approach and found  
26 91,275 DMRs, with an average length of 453 base pairs (bp). Principal component analysis (PCA)  
27 of the methylation density measured across all DMRs revealed global tissue-specific clustering,  
28 with three heterogeneous clusters representing blood, gut and a diverse group of other solid organ  
29 tissues (**Fig.1d, Supplemental Fig. 1**). To identify both global and local structural features within  
30 reference methylomes, we applied uniform manifold approximation projection (UMAP)<sup>24</sup>. We  
31 found that UMAP further resolves reference methylation profiles into clusters comprised of  
32 specific cell-types (**Fig. 1d,e**). For example, among myeloid cells, cell types with similar lineages  
33 such as macrophages and monocytes clustered more closely than those from other lineages on  
34 the UMAP projection. These analyses confirm that genome-wide methylation profiles are cell,  
35 tissue and organ-type specific, and can in principle inform its tissue of origin, as described  
36 previously<sup>7,8,25-27</sup>.

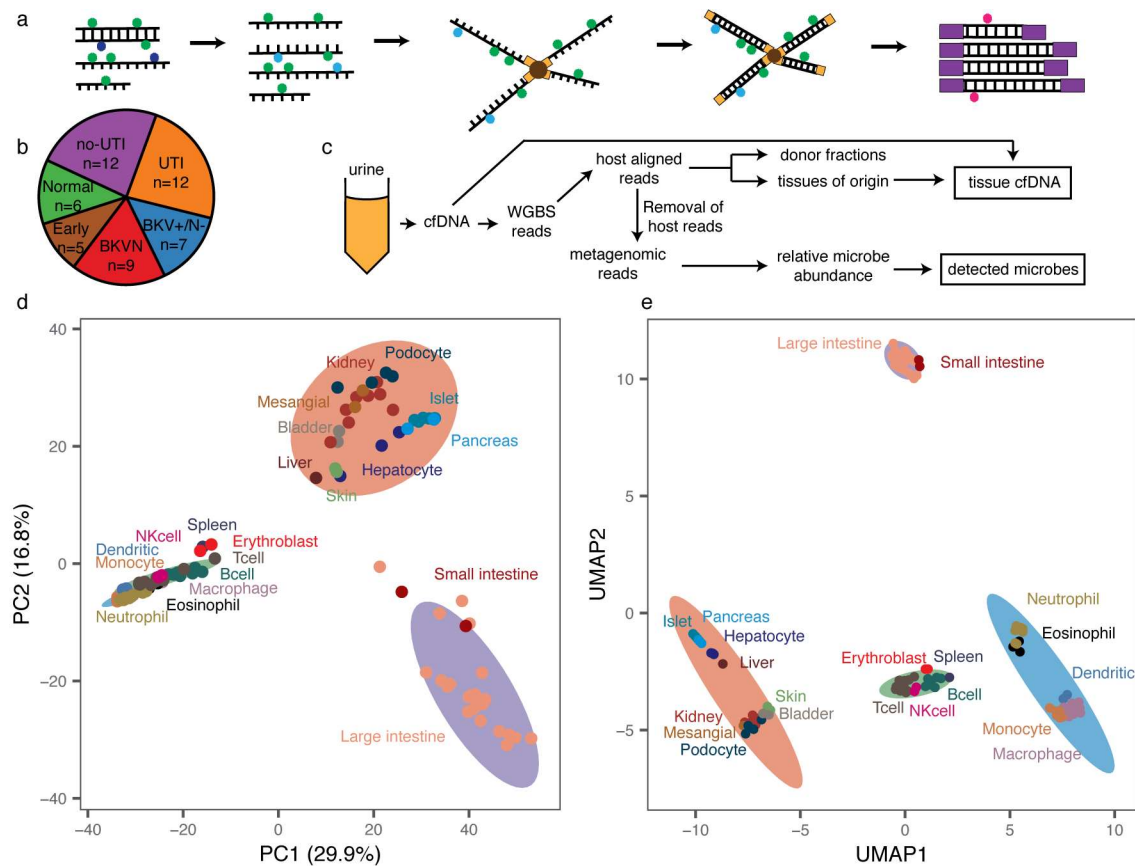


**Figure 1. Study methodology and cell type specificity of genome-wide methylation profiles.** **a** Schematic of single-stranded library preparation method. cfDNA is denatured and treated with sodium bisulfite, which converts unmethylated cytosines (dark blue) into uracils (light blue) but not methylated cytosines (green). Bisulfite-treated DNA is first ligated to single-stranded adapters and bound to magnetic beads. Second-strand synthesis, and double-stranded adapter ligation are performed on the beads. The final step is a PCR, which converts uracils to thymines (red). **b** Pie chart with summary of samples included in this study, colored by pathology. **c** Schematic of WGBS analysis workflow. **d** Principal component analysis of reference whole-genome methylation profiles from human tissues. **e** Uniform manifold approximation projection of reference methylation profiles. Ellipses in **d**, **e** are normal 95% confidence ellipses (K-means, 4 centers).

1

## 1 Cell-free DNA origin associated with infection

2  
3 To determine methylation marks comprised within urinary cfDNA, we first aligned the WGBS  
4 reads to a human reference genome via bwa-meth<sup>28</sup>. We quantified the efficiency of bisulfite  
5 conversion achieved in experiments from the fraction of reported methylated C[A/T/C] base pairs,  
6 which are rarely methylated in humans<sup>29</sup>. We found a conversion efficiency greater or equal to  
7 94.5% for all cfDNA isolates (see Methods). We next projected the genome-wide cfDNA CpG  
8 methylation profiles onto the two-dimensional feature spaces generated by PCA and UMAP for  
9 the 112 public references. We found that cfDNA profiles organized between the cluster that  
10 comprised kidney tissue and the white blood cell cluster on the PCA and UMAP two-dimensional  
11 projections (**Fig. 2 a,b**). This observation provided a first indication that urinary cfDNA originates  
12 primarily from blood cell types and kidney tissue. Other cell types found in the urinary tract  
13 contributed less significantly to urinary cfDNA.

14  
15 We next computed the proportion of transplant donor-derived cell-free DNA (ddcfDNA) in these  
16 samples. We and others have identified ddcfDNA as a non-invasive, quantitative marker of graft  
17 injury in solid-organ transplantation<sup>2,4,30,31</sup>. For sex-mismatched donor-recipient pairs, the  
18 proportion of ddcfDNA can be estimated by evaluating the coverage of the Y chromosome relative  
19 to the autosomal chromosomes (see Methods)<sup>2,32</sup>. We verified that the proportion of ddcfDNA  
20 measured by sequencing of bisulfite-treated cfDNA matched the proportion of ddcfDNA measured  
21 using conventional sequencing (n=36 matched samples, Spearman's rho = 0.97, p-value <  
22  $2.2 \times 10^{-16}$ , see Methods, **supplemental figure 2**), and then quantified the proportion of ddcfDNA  
23 in urine for all sex-mismatched donor-recipient transplant pairs (n=46). We observed a very large  
24 range of ddcfDNA values across all samples (3%-99%). Superimposing the ddcfDNA proportion  
25 on the PCA and UMAP projections revealed that samples with a higher proportion of ddcfDNA  
26 landed closer to the reference cluster comprised of kidney tissue (**Fig. 2a,b**, n=44, two samples  
27 from a patient that received both a kidney and bone marrow transplant were excluded from this  
28 analysis, because the donor fraction represents the summation of kidney DNA and engrafted  
29 bone marrow-derived cells for this case). This observation provided a second line of evidence  
30 that urinary cfDNA is a mixture of cfDNA derived from blood cell types and kidney tissue.

31  
32 To quantify the contributions of different tissues to the mixture of cfDNA in urine, we implemented  
33 quadratic programming. Quadratic programming retrieves the fractional contribution of each  
34 tissue,  $\pi_i$ , from the ensemble cfDNA methylation profile  $Y$ , and the public reference methylation  
35 profile for each tissue,  $X_i$ :  $Y = \pi_i X_i + \epsilon$ , where  $\epsilon$  is an error term (see Methods)<sup>33</sup>. Using this approach,  
36 we found an excellent quantitative agreement (Spearman's rho=0.88, p-value <  $2.2 \times 10^{-16}$ , **Fig.**  
37 **2c**) between the proportion of kidney specific cfDNA (determined from methylation marks) and  
38 ddcfDNA (determined from genetic marks in cfDNA) for sex-mismatched donor-recipient  
39 transplant pairs (n=44). This analysis provided support for the use of our bioinformatic and  
40 molecular approaches to quantify the tissue and cell types of origin of cfDNA in urine.

41  
42 We proceeded to analyze the relative contributions of all cell and tissue types comprised within  
43 the pure cell and tissue references against clinical tests of infection. We found that the cfDNA cell  
44 and tissue composition was associated with infection status (**Fig. 2d**). For example, the relative

1 contribution of kidney-derived cfDNA was elevated in samples from patients with BKV infection  
 2 compared to patients diagnosed with bacterial UTI (p-value =  $2.0 \times 10^{-4}$ , mean of 48.6%; mean  
 3 12.5%, respectively, **Fig. 2d**). We further found that leukocytes were enriched in samples from  
 4 patients diagnosed with bacterial UTI by conventional culture, and that neutrophils are the main  
 5 contributors to the differences in white blood cell content, as expected from their role as first  
 6 responders to infection (**Fig. 2d**)<sup>34</sup>.  
 7

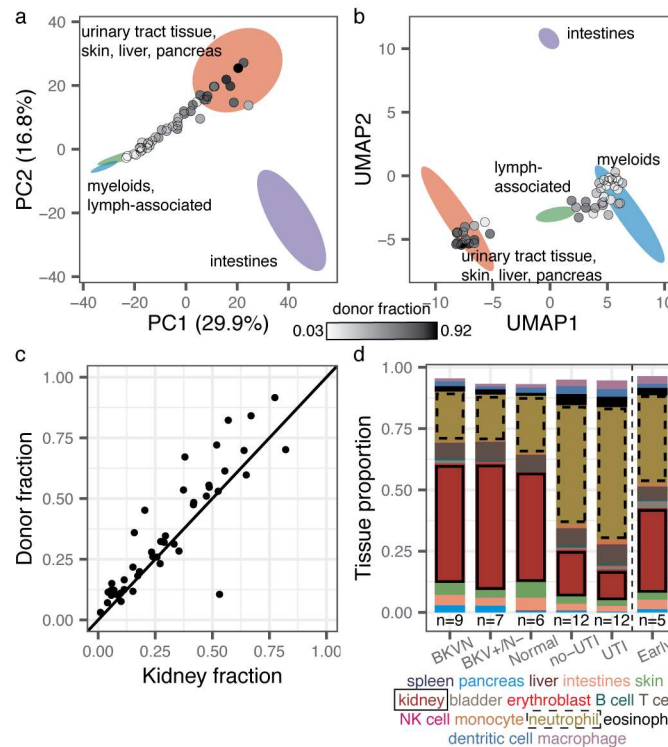


**Figure 2. Methylation marks within cfDNA inform its tissues-of-origin.** **a, b** Projection of cfDNA genome-wide methylation profiles onto PCA and UMAP feature space (from Fig. 1d,e). Data points colored according to donor fraction (n=44). **c** Comparison of the proportion of kidney-derived cfDNA and donor-derived cfDNA measured for sex-mismatched donor-recipient pairs (n=44). Spearman's rho=0.88, p-value <  $2.2 \times 10^{-16}$ . Samples from dual bone-marrow and kidney transplants are excluded. **d** Barplot of cfDNA cell and tissue type composition measured for clinical groups.



1 The relative proportion of cfDNA from a specific tissue is a function of the proportion of DNA  
2 released from all other cell types or tissues and may therefore be a convoluted measure of tissue-  
3 specific injury. To overcome this limitation, we computed the absolute concentration of tissue-  
4 specific cfDNA by multiplying the proportion of tissue and cell type specific DNA obtained using  
5 the approaches above with the concentration of total host-derived cfDNA in the sample (see  
6 Methods). We observed marked temporal dynamics of the concentration of cfDNA from different  
7 cell and tissue types in absence of infection (no-UTI, Normal and Early groups, **Fig. 3a**). Recovery  
8 of postoperative stress in the first three days after transplantation was associated with a marked  
9 increase in cfDNA from most tissues. This signal of early post-operative injury decayed to a low  
10 baseline within 10 days after transplantation, and after three months post transplantation  
11 quiescence was observed with markedly low amount of cfDNA from all cell and tissue types in  
12 absence of infection.

13  
14 We examined whether the cfDNA concentration of certain tissues was associated with infection  
15 pathology. We first examined all samples from patients that were screened for BKVN via needle  
16 biopsy (all samples collected after day 100). We observed marked differences in the concentration  
17 of kidney-derived cfDNA for samples from patients diagnosed with BKVN (BKVN vs Normal, mean  
18 kidney cfDNA 21.9 ng/ml, and 1.5ng/ml, respectively p-value =  $4.0 \times 10^{-4}$ , **Fig. 3b**), indicating  
19 significant tissue injury associated with BKVN. In addition, we found that this cfDNA measurement  
20 can distinguish BKVN from BKV reactivation without nephropathy (BKVN vs BKV+/N-, mean  
21 kidney cfDNA 21.9 ng/ml and 6.9 ng/ml, respectively, p-value =  $7.9 \times 10^{-3}$ ), and BKV+/N- from  
22 Normal (mean kidney cfDNA 6.9 ng/ml and 1.5ng/ml, respectively, p-value =  $1.2 \times 10^{-3}$ ). The  
23 concentration of leukocyte cfDNA was elevated in urine from patients diagnosed with BKVN  
24 (mean 19.0 ng/ml vs. 1.9 ng/ml in Normal, p-value =  $2.8 \times 10^{-3}$ ) and BKV+/N- (mean 4.0 ng/ml vs.  
25 1.9 ng/ml, p-value =  $3.5 \times 10^{-2}$ ) but could not distinguish BKVN from BKV reactivation without  
26 nephropathy (p-value =  $5.5 \times 10^{-2}$ ) (**Fig. 3c**). Together these experiments point to the utility of the  
27 assay presented here to non-invasively distinguish nephropathy and inflammation due to BK virus  
28 infection. The kidney cfDNA concentration in samples collected from patients within the first three  
29 days after transplantation, a period during which we observed significant post-operative injury  
30 (**Fig. 3a**), was also elevated (12.4 ng/ml) and could not be differentiated from the concentration  
31 measured in samples from patients with BK disease (p-value=0.30 and 0.20 when compared to  
32 BKVN and BKV+/N-, respectively). This last observation underlines the importance of paired  
33 metagenomic evaluation to distinguish infection and non-infection related host injury.

34  
35 We next evaluated all samples from patients that were screened for UTI via conventional urine  
36 culture (no-UTI group and UTI group, n=12 each). These samples were collected between days  
37 8 and 55 post-transplant, a period in which we observed significant host injury in absence of  
38 infection (**Fig. 3a**), and were evaluated for hematuria by microscopy, a clinical marker of injury.  
39 We found that both bladder and leukocyte-derived cfDNA were elevated in samples from patients  
40 diagnosed with bacterial UTI and hematuria (Red Blood Cell [RBC] counts per High Power Field  
41 [HPF] greater than 4) compared to patients diagnosed with UTI in the absence of hematuria (**Fig.**  
42 **3d**, receiver operator characteristic analysis, area under the curve [AUC] = 0.91 for bladder  
43 cfDNA). We further found correlations between red blood cell (RBC) counts and the  
44 concentrations of bladder cfDNA in urine (all samples for which RBC per HPF was measured,

1 n=24, Spearman's rho = 0.43, p-value =  $3.5 \times 10^{-2}$ ). Together, these observations demonstrate the  
2 utility of our assay to assess the severity of injury due to bacterial UTI. The performance of the  
3 concentration of bladder cfDNA in distinguishing bacterial UTI and absence of UTI with and  
4 without hematuria was modest (AUC = 0.64 for bladder cfDNA, **Fig. 3d**), which is likely explained  
5 by the significant non-infection related injury in this patient population in the sample time window.  
6

7 Last, we asked whether the concentration of kidney derived cfDNA correlated with serum  
8 creatinine, a clinical marker of kidney function. Creatinine is a waste product of muscle  
9 metabolism and elevated serum creatinine levels are an indication of poor kidney function. We  
10 found good agreement between kidney-specific cfDNA in urine and serum creatinine (all samples  
11 for which serum creatinine was measured, n = 50, Spearman's rho=0.51, p-value= $1.5 \times 10^{-4}$ ).  
12 Together, the data presented in Figure 3 provide strong support for the use of WGBS of cfDNA  
13 to quantify host injury due to viral and bacterial UTI.  
14

15 The pattern of degradation of cfDNA in plasma has previously been shown to depend on their  
16 origin and pathology. For example, tumor-derived cfDNA was found to be significantly shorter  
17 than cfDNA from normal tissue<sup>35,36</sup>. Here, we sized urinary cfDNA using paired-end read mapping  
18 (see Methods). Bisulfite treatment is known to lead to DNA degradation<sup>37</sup>, and this was  
19 corroborated by our cfDNA sizing assay. We found that bisulfite-treated cfDNA is on average 10.1  
20 bp shorter than untreated cfDNA (n = 38 matched samples). We furthermore found that the mean  
21 fragment length of host-derived cfDNA was negatively correlated with the white blood cell  
22 proportion (Spearman's rho = -0.45, p-value =  $1.1 \times 10^{-3}$ , n=51) and was shorter for samples from  
23 patients with bacterial infection than from patients without bacterial UTI (p-value =  $2.4 \times 10^{-2}$ , mean  
24 length of 93 and 101bp, respectively, **Fig. 3f, Supplemental Fig. 3**). This observation is in line  
25 with previous reports that leukocytes create a degradative environment for DNA<sup>38,39</sup>. The fragment  
26 size profile of cfDNA may offer an additional metric by which patients with different infectious  
27 pathologies can be stratified.  
28



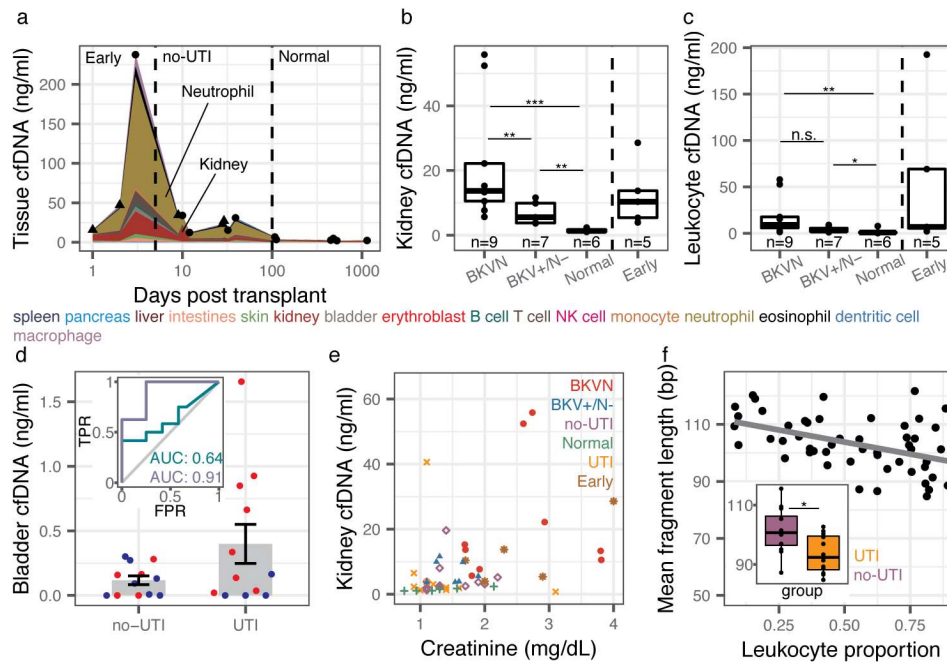


**Figure 3. Cell-type deconvolution of urinary cfDNA reveals host response to infection.**  
**a** Concentration of tissue-specific cfDNA for samples with no clinical indication of infection (triangles indicate mean for multiple measurements at the same time point, single samples indicated with circles). **b,c** Kidney (b) and leukocyte (c) cfDNA concentration for BKVN, BKV+/N-, Normal and Early groups. **d** Bladder cfDNA concentration for no-UTI and UTI groups. Inset shows receiver operating characteristic analysis of the performance of bladder cfDNA in distinguishing no-UTI from UTI groups (blue) and in distinguishing hematuria (RBC per HPF >4) from no hematuria (RBC per RBC ≤4) in samples from the UTI group. **e** Serum creatinine versus kidney urinary cfDNA concentration (n=50). Spearman's rho=0.51 p-value=1.4x10<sup>-4</sup>. **f** Mean host cfDNA fragment length versus leukocyte proportion (n=51). Spearman's rho=-0.45, p-value=1.1x10<sup>-3</sup>. Inset shows boxplots of fragment lengths measured for the UTI and no-UTI groups. Boxplot features detailed in the Methods section. \* p-value < 0.05, \*\* p-value < 0.01, \*\*\* p-value < 0.001.

1  
2  
3  
4  
5  
6  
7  
8  
9  
10  
11  
12  
13

### Whole genome bisulfite sequencing of cfDNA identifies clinically-relevant pathogens

Bisulfite conversion of DNA followed by PCR converts unmethylated cytosines into thymines. A corollary of bisulfite treatment is a decrease in cytosine content, and a reduction in overall read complexity. To determine whether WGBS can be used to identify specific uropathogens despite the reduction in sequence complexity inherent to bisulfite conversion, we compared pathogen abundances measured after shotgun sequencing of bisulfite-treated and untreated cfDNA (matched samples, n=38). We determined the relative representation of bacteria and viruses in these datasets, using approaches previously described<sup>2,3,40</sup> (see Methods). We computed the representation of microbial genomes relative to human genome copies and expressed this quantity as relative genome equivalents (RGE, see Methods). Figure 4a shows a close

1 quantitative agreement between the species abundance measured for bisulfite-treated and  
2 untreated cfDNA, confirming that it is possible to broadly identify microbial cfDNA via shotgun  
3 sequencing of bisulfite-treated cfDNA (**Fig. 4a**, Spearman's rho = 0.72, p-value <  $2.2 \times 10^{-16}$ ).

4  
5 We assessed the relative genomic abundance of cfDNA from bacterial and viral pathogens  
6 identified by conventional diagnostic assays. In 9 out of 9 BKVN samples and 6 out of 7 BKV+/N-  
7 samples, we identified high BK viral loads (RGE >  $10^3$ , **Fig. 4b**). These values correlated strongly  
8 with matched plasma BKV copies as determined by quantitative PCR (Spearman's rho=0.81, p-  
9 value= $6.2 \times 10^{-6}$ ). We next compared the relative genomic abundance of bacterial cfDNA for  
10 patients diagnosed with bacterial infection (12 samples matched with a positive clean-catch  
11 midstream urine culture, UTI group), to the relative genomic abundance measured for 12 negative  
12 clean-catch midstream urine cultures (no-UTI group). Of these positive urine cultures, 11 had a  
13 single identifiable bacterium (*Escherichia coli*, n=4; *Enterococcus faecalis*, n=3; *Pseudomonas*  
14 *aeruginosa*, n=2; *Enterococcus faecium*, n=1; *Klebsiella oxytoca*, n=1), while a single sample  
15 presented 2 different bacterial species (*E. faecalis* and coagulase-negative Staphylococcus). We  
16 found agreement between the urinary cfDNA assay described here and conventional bacterial  
17 culture (detection accuracy = 100%, no information rate = 16.0%, p-value [accuracy > no  
18 information rate] <  $2.2 \times 10^{-16}$ , **Fig. 4c**). These results support the use of WGBS of cfDNA as an  
19 assay to screen for potential pathogens in clinical isolates.

20  
21 Finally, we tested whether the cfDNA cell and tissue-type composition depended on the presence  
22 or absence of viral and bacterial pathogens as determined by WGBS. We used unsupervised  
23 hierarchical clustering of the cfDNA cell and tissue type composition for all samples in which BK  
24 virus (RGE >  $10^3$ ) or a potential bacterial uropathogen was detected (RGE > 0.09, the lowest  
25 corresponding relative genomic abundance observed in the comparison to clinical metrics  
26 described above). This analysis, shown in figure 4d, summarizes the major layers of information  
27 that are made accessible with the cfDNA assay reported here, and shows that the cfDNA tissue  
28 and cell type composition is associated with the presence or absence of viral or bacterial  
29 uropathogens.

30  
31

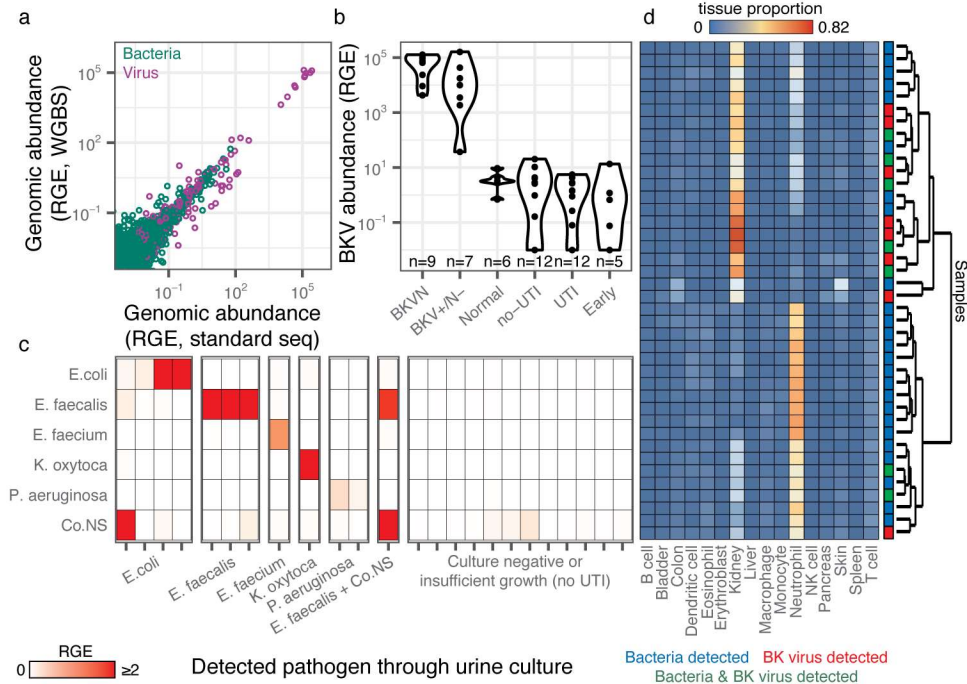


**Figure 4. WGBS of microbial cfDNA for clinical pathogen identification.** **a** Scatterplot of relative genomic abundance of bacteria (green) and viruses (purple) measured by WGBS and conventional cfDNA sequencing. Spearman's rho = 0.72, p-value < 2.2x10<sup>-16</sup>. Each data point represents the genomic abundance of a single microbe in matched bisulfite and untreated urinary cfDNA. **b** Violin plots of BKV sequence abundance in all samples. **c** Relative genomic abundance of microbes identified through urine culture. **d** Heatmap of tissue proportions in samples where a microbe was detected through WGBS. Rows are hierarchically clustered according to tissue composition.

## DISCUSSION

We have described a metagenomic assay that simultaneously quantifies the abundance of a large array of viruses and bacteria in clinical samples, and the degree of host injury. This work is motivated by the need to integrate information about host-microbe interactions in clinical metagenomic assays in order to distinguish infection from infectious disease, and to assess the severity of disease. The assay reported here takes advantage of genome-wide profiling of CpG methylation marks comprised within cfDNA to quantify the contributions of different cell and tissue types to the mixture of cfDNA in the sample, and thereby the degree of host damage. Compared to conventional metagenomic cfDNA assays<sup>2,41</sup>, this assay requires a single additional experimental step, bisulfite treatment of the cfDNA isolate, which is inexpensive and can be completed within approximately two hours.

We tested the utility of this assay to monitor viral and bacterial infections of the urinary tract in a cohort of kidney transplant recipients. We found that the concentration of cfDNA derived from

1 different cell and tissue types was a function of infection status in these patients. Patients  
2 diagnosed with BKVN had elevated kidney-specific cfDNA in urine compared to a Normal control  
3 group. BKV reactivation without nephropathy was also characterized by elevated levels of kidney-  
4 specific DNA but not to the same degree as BKVN. Our findings suggest that there may be kidney  
5 damage occurring before the onset of nephropathy. Biopsies only provide information on the  
6 sampled region of the kidney, and do not capture the inherent heterogeneity of BKV infection  
7 within the kidney allograft and disease progression. The assay described here may find use as a  
8 noninvasive alternative to conventional biopsy to screen for BKV related kidney injury.

9  
10 In addition, patients with bacterial UTIs show higher neutrophil contributions, suggesting immune  
11 activation and recruitment of neutrophils to the urinary tract, as well as elevated amounts of  
12 bladder cfDNA, indicating tissue injury. A common question in infectious diseases is how to  
13 interpret positive urine cultures. Outside of specific indications such as pregnancy, urological  
14 procedures, and being within 3 months of transplant<sup>42,43</sup>, a positive urine culture is currently  
15 treated with antibiotics only in symptomatic individuals. By quantifying the release of cfDNA from  
16 different cell types and tissues, the assay reported here can provide clinicians with additional  
17 information to guide treatment decisions.

18  
19 A quantitative measurement of the tissues-of-origin of cfDNA constitutes a generalizable  
20 noninvasive approach to identify injury to vascularized tissues and participation of the immune  
21 system and can find wide application in diagnostic medicine. Several studies have reported  
22 technologies to trace the tissue origin of cfDNA in wide range of settings, targeting different  
23 epigenetic marks comprised within cfDNA, including the footprints of nucleosomes and  
24 transcription factors, cytosine methylation and hydroxymethylation<sup>7-9,44,45</sup>. Here, we have applied  
25 this technology for the first time to the monitoring of host tissue damage due to infection.

26 Host-based molecular signatures have previously been considered as classifiers of infectious  
27 complications. In respiratory infection, host transcriptional profiling of the peripheral blood has  
28 been shown to provide a means to characterize the host response to viral and bacterial infection,  
29 and to discriminate between infectious and noninfected states<sup>46</sup>. Host-response molecular  
30 signatures thereby offer a diagnostic approach orthogonal to approaches that focus on viral and  
31 bacterial pathogens. Recently, Langelier et al. described a diagnostic approach that combines  
32 transcriptional profiling and metagenomic sequencing of tracheal aspirate to classify lower  
33 respiratory tract infection<sup>47</sup>. Here, we show that a cfDNA assay can be used to screen for  
34 infectious agents and to quantify the degree of host damage. The strength of this assay lies in its  
35 simplicity of implementation, its noninvasiveness, and its ability to directly interrogate host  
36 damage, the metric that is most relevant to classify infectious complications in the framework  
37 proposed by Casadevall and Pirofski<sup>5</sup>.

38  
39 In summary, we propose that WGBS of cfDNA can be used as a metagenomic sequencing assay  
40 to provide in depth understanding of both the metagenome as well as the host response to  
41 infection. This assay is generalizable to multiple diseased states and has the potential to  
42 distinguish colonization from infectious disease in a clinical setting.

43  
44

## 1 MATERIALS AND METHODS

2

3 **Study cohort.** 51 urine samples were collected from 36 kidney transplant recipients treated at  
4 NewYork-Presbyterian Hospital-Weill Cornell Medical Center. The study was approved by the  
5 Weill Cornell Medicine Institutional Review Board (protocols 9402002786 and 710009490 and  
6 1207012730). All patients provided written informed consent.

7

8 Twenty-two urine samples from 21 patients were collected at the time of kidney allograft biopsy;  
9 9 samples were collected from patients with BK viremia were found to have BK polyomavirus  
10 nephropathy with positive immunohistochemical staining for SV40 large T antigen (BKVN), 7  
11 samples from patients with BK viremia were found not to have BK polyomavirus nephropathy  
12 (BKV+/N-) and 6 patients did not have BK viremia and had no significant pathology in the biopsies  
13 (Normal).

14

15 Plasma BKV copies per ml of blood were measured using the quantitative assay developed by  
16 Quest Diagnostics® as part of clinical testing.

17

18 Renal Allograft Biopsy Evaluation: Percutaneous core needle biopsy specimens of kidney  
19 allografts were fixed in 10% buffered formalin and embedded in paraffin. Tissue sections were  
20 stained with hematoxylin eosin, periodic acid Schiff, periodic acid silver methenamine, and  
21 Masson trichrome for light microscopic evaluation. Routine immunofluorescence staining of fresh  
22 frozen biopsy tissue and immunoperoxidase staining of paraffin-embedded biopsy tissues were  
23 performed using standard techniques to detect the presence of positive staining for C4d (Fisher  
24 Scientific – C4d polyclonal NC9575575; Quidel – C4d monoclonal Cat. No. A213) and SV40 large  
25 T antigen of the BK virus (Affinity purified and agarose conjugated IgG2A mouse monoclonal  
26 antibody recognizing the 94kDa SV40 large T antigen; PAb416, Cat. No. DPO2, Calbiochem,  
27 USA) respectively.

28

29 Twenty-four urine samples were collected from patients who underwent same day urine culture<sup>2</sup>.  
30 Briefly, urine samples were plated on tryptic soy agar with sheep blood and incubated at 35C.  
31 Samples were classified as UTI positive (UTI, n=12) if an organism was detected at least at the  
32 genus level with 10,000 colony forming units (cfu) per ml. Samples were classified as UTI negative  
33 (no-UTI, n=12) if no organism was isolated (n=11), or if no organism was identified at the genus  
34 level and the colony counts was under 10,000 cfu/ml (n=1). Early time point (n=5) and Normal  
35 (n=6) samples were selected from patients who did not present symptoms for BK polyomavirus  
36 or UTI and who provided a urine sample within three days, or following 100 days after  
37 transplantation, respectively. Normal samples were collected from patients who underwent  
38 routine biopsy as part of standard clinical practice and did not show histological evidence of  
39 inflammation or nephropathy.

40

41 **Urine collection, supernatant isolation and cfDNA extraction.** Urine was collected using a  
42 conventional clean-catch method (n=46) or through foley catheter (n=5). Approximately 50 ml of  
43 urine was centrifuged at 3,000g for 30 minutes on the day of collection and supernatants were  
44 stored at -80C. cfDNA was extracted from 1 or 4 ml of urine according to manufacturer



1 recommendations (Qiagen Circulating Nucleic Acid Kit, Qiagen, Valencia, CA) and quantified  
2 using a Qubit fluorometer 3.0 (high sensitivity double-stranded DNA kit, ThermoFisher, Waltham,  
3 MA). The concentration of cfDNA in the sample was calculated by multiplying the measured  
4 concentration of DNA in eluant by the elution volume and dividing by the volume of the urine  
5 sample.

6  
7 **Bisulfite treatment, library preparation and Illumina sequencing.** Between 5 and 20  $\mu$ l of  
8 eluted cfDNA was bisulfite-treated using the Zymo EZ DNA methylation kit according to  
9 manufacturer's recommendations (Zymo EZ DNA methylation kit, Irvine, CA). Samples were  
10 eluted in approximately 30  $\mu$ l. Samples were prepared for sequencing using a single-stranded  
11 library preparation<sup>16,17</sup>. Libraries were characterized using DNA fragment analysis (Advanced  
12 Analytical Fragment Analyzer) and sequenced (Illumina NextSeq550, 2x75bp).

13  
14 **Alignment to the human genome and methylation extraction.** Low-quality bases and adapter  
15 sequences were trimmed (Trimmomatic v-036<sup>48</sup>). Reads were aligned to a C-to-T converted hg19  
16 reference using bwa-meth v0.2.0<sup>28</sup>. PCR duplicates and low quality reads were removed using  
17 Samtools v1.16<sup>49</sup>. Methylation densities were measured using MethylDackel v.0.3.0-3-  
18 g094d926<sup>50</sup>.

19  
20 **Quantification of urine-derived microbial cfDNA.** The burden of microbial cfDNA after  
21 conventional sequencing was determined as previously described<sup>3</sup>. The burden of microbial  
22 cfDNA after WGBS was determined using a similar approach. Briefly, low-quality bases and  
23 adapter-specific sequences were trimmed (Trimmomatic<sup>48</sup>, v036) and short reads were merged  
24 (FLASH<sup>51</sup> v1.2.11). Reads were aligned to a C-to-T converted hg19 reference using bwa-meth<sup>28</sup>  
25 (v0.2.0) and to the standard hg19 genome using bwa<sup>49</sup> (v.0.7.13-r1126) to remove converted and  
26 unconverted host reads. Reads were then BLASTed<sup>52</sup> to a list of C-to-T converted microbial  
27 reference genomes, and a relative abundance of each organism was determined using  
28 GRAMMy<sup>40</sup>. The fraction of reads of microbial origin was defined as the ratio of reads mapping to  
29 a microbial reference to the total number of paired-end reads for that sample.

30  
31 **Bisulfite conversion efficiency.** Although CpG dinucleotides are often methylated in the human  
32 genome, C[A/T/C] molecules are rarely methylated. We estimated bisulfite conversion efficiency  
33 by calculating the reported rate of C[A/T/C] methylation using MethPipe v.3.4.3<sup>53,54</sup>.

34  
35 **Donor fraction measurement.** Donor-specific cfDNA was measured in sex-mismatched donor-  
36 recipient pairs as previously described<sup>2</sup> by first adjusting sequence mappability with HMMcopy<sup>55</sup>.

37  
38 **Cell and tissue methylation reference preparation.** References made available by public  
39 consortia were downloaded (Supplemental table 1, refs). Genomic coordinates of references  
40 aligned to hg38 assembly of the human genome were converted to the hg19 assembly using  
41 CrossMap<sup>56</sup>. Single base pair CpG methylation values (forward strand) were extracted, and all  
42 references were merged by genomic coordinates using BEDTools<sup>57</sup>. Methylation profiles were  
43 grouped by tissue-type, and differentially methylated regions (DMRs) were found using  
44 approaches implemented in Metilene (difference  $\geq$  20%, q-value  $<$  0.05)<sup>23</sup> in a one-versus-one



1 approach. Overlapping regions were merged, and tissue methylation profiles were averaged over  
2 those regions. Regions were constrained to having a minimum of 10 CpGs per regions, with at  
3 least 1 CpG per 100 base pairs.

4  
5 **Tissues-of-origin deconvolution.** Tissues and cell-types of origin were determined by quadratic  
6 programming<sup>58,59</sup> according to the following equation:

7  
8 
$$\min \|Ax - b\|^2 \text{ subject to } x_i \geq 0 \forall x_i \in x \text{ and } \sum x \leq 1$$

9  
10 Where A is an  $(m+1) \times n$  matrix with m cell and tissue methylation references spanning n DMRs.  
11 The additional column contains an error parameter to consider potential missing references, non-  
12 tissue specific methylation, and other sources of error.  $x_i$  represents the contribution of each tissue  
13 to the cfDNA mixture. b is a  $1 \times n$  vector of the observed methylation. Only autosomal  
14 chromosomes were considered for tissue of origin measurements. The absolute concentration of  
15 tissue specific cfDNA in the samples was calculated by multiplying the tissue proportion by the  
16 absolute cfDNA concentration of the sample and by the fraction of sequenced reads of human  
17 origin.

18  
19 **Dimensional reduction.** Dimensional reduction was performed on DMRs selected in the  
20 reference that were present in all samples. Clustering was performed using PCA (R, prcomp  
21 package) and UMAP (R, umap package). Default UMAP parameters were used (15 neighbors, 2  
22 components, Euclidean metric and a minimum distance of 0.1). Sample methylation profiles were  
23 projected onto the two-dimensional feature spaces of PCA and UMAP using the predict function  
24 in R.

25  
26 **Microbe detection through sequencing.** For each culture-detected microbe (*E. coli*, *E. faecalis*,  
27 *E. faecium*, *P. aeruginosa*, *K. oxytoca* and coagulase-negative *Staphylococcus*), a specific  
28 threshold corresponding to the smallest relative genomic abundance with positive culture was  
29 used to classify all tested samples. Samples were classified as being positive (RGE [tested  
30 microbe]  $\geq$  minimum threshold [tested microbe]) or negative for each culture-detected microbe  
31 (RGE [tested microbe]  $<$  minimum threshold [tested microbe]), and a confusion matrix was used  
32 to compare predicted values through sequencing with reference values determined by urine  
33 culture. Test accuracy statistics were calculated using R (caret package). Samples were classified  
34 as virus and/or bacteria positive if the relative genomic of a microbe was greater than set  
35 thresholds ( $10^3$  for BK virus, 0.09 for bacteria) and if the microbe is not a known sequencing  
36 contaminant<sup>60</sup> (common sequencing contaminants that are also known uropathogens were  
37 classified as positive).

38  
39 **Statistical analysis.** All statistical methods were performed in R (v.3.5). All groups were  
40 compared using a two-sided Wilcoxon test (R stats package). Boxes in the boxplots indicate the  
41 25th and 75th percentiles, the band in the box indicates the median, lower whiskers extend from  
42 the hinge to the smallest value at most  $1.5 \times$  IQR of the hinge, and higher whiskers extend from

1 the hinge to the highest value at most 1.5× IQR of the hinge. Violin plots are bound by density  
2 estimates of the data distribution.

3

4 **Data availability.** The sequencing data generated for this study will be made available in the  
5 database of Genotypes and Phenotypes (dbGaP).

6

7 **Code availability.** All custom scripts are available at  
8 [https://github.com/alexpcheng/bisulfite\\_cfDNA](https://github.com/alexpcheng/bisulfite_cfDNA)

9

10 **Materials and Correspondence.** All requests should be submitted to I.D.V.  
11 (vlaminck@cornell.edu) and D.D. (dmd2001@med.cornell.edu).

12

### 13 **Supplementary Materials.**

14 **Figure S1.** Principal component analysis of reference methylomes.

15 **Figure S2.** Scatterplot of corresponding donor fractions in sex-mismatched samples that  
16 underwent both WGBS and standard sequencing.

17 **Figure S3.** Mean fragment length of bisulfite-treated cfDNA for BKVN, BKV+/N-, Normal, no-UTI,  
18 UTI and Early groups.

19 **Table S1.** Reference methylation dataset metadata

20 **Table S2.** Clinical information of urine samples

21

### 22 **COMPETING FINANCIAL INTERESTS**

23 The authors declare no competing financial interests.

24

### 25 **AUTHOR CONTRIBUTIONS**

26 A.P.C., P.B., M.P.C., J.R.L., D.D., M.S., and I.D.V. contributed to the study design. A.P.C.  
27 performed the experiments. A.P.C., P.B., J.R.L., D.D., and I.D.V. analyzed the data. A.P.C.,  
28 M.P.C., D.D., J.R.L., and I.D.V. wrote the manuscript. All authors provided comments and edits.

29

### 30 **ACKNOWLEDGMENTS**

31 We thank Peter Schweitzer and colleagues at the Cornell Biotechnology Resource Center (BRC)  
32 for help with sequencing assays. This work was supported by US National Institute of Health (NIH)  
33 grant 1DP2AI138242 to IDV, US NIH, grant 1R21AI133331 to IDV and JRL, a National Sciences  
34 and Engineering Research Council of Canada (401236174) fellowship to APC, and a National  
35 Science Foundation Graduate Research Fellowship Program (NSF-GRFP) grant DGE-1144153  
36 to PB.

37

38

## REFERENCES

1. Weber, G., Shendure, J., Tanenbaum, D. M., Church, G. M. & Meyerson, M. Identification of foreign gene sequences by transcript filtering against the human genome. *Nat. Genet.* **30**, 141–142 (2002).
2. Burnham, P. *et al.* Urinary cell-free DNA is a versatile analyte for monitoring infections of the urinary tract. *Nat. Commun.* **9**, 2412 (2018).
3. De Vlaminck, I. *et al.* Temporal response of the human virome to immunosuppression and antiviral therapy. *Cell* **155**, 1178–87 (2013).
4. De Vlaminck, I. *et al.* Noninvasive monitoring of infection and rejection after lung transplantation. *Proc. Natl. Acad. Sci. U. S. A.* **112**, 13336–41 (2015).
5. Casadevall, A. & Pirofski, L. A. Host-pathogen interactions: basic concepts of microbial commensalism, colonization, infection, and disease. *Infect. Immun.* **68**, 6511–8 (2000).
6. Casadevall, A. & Pirofski, L. Host-Pathogen Interactions: Redefining the Basic Concepts of Virulence and Pathogenicity. *Infect. Immun.* **67**, 3703 LP-3713 (1999).
7. Sun, K. *et al.* Plasma DNA tissue mapping by genome-wide methylation sequencing for noninvasive prenatal, cancer, and transplantation assessments. *Proc. Natl. Acad. Sci. U. S. A.* **112**, E5503-12 (2015).
8. Lehmann-Werman, R. *et al.* Identification of tissue-specific cell death using methylation patterns of circulating DNA. *Proc. Natl. Acad. Sci. U. S. A.* **113**, E1826-34 (2016).
9. Lehmann-Werman, R. *et al.* Specific detection of cell-free DNA derived from intestinal epithelial cells using methylation patterns. *bioRxiv* (2018).
10. Wilson, M. R. *et al.* Actionable diagnosis of neuroleptospirosis by next-generation sequencing. *N Engl J Med* **370**, 2408–2417 (2014).
11. Blauwkamp, T. A. *et al.* Analytical and clinical validation of a microbial cell-free DNA sequencing test for infectious disease. *Nat. Microbiol.* (2019). doi:10.1038/s41564-018-0349-6
12. 2016 Activity data Report - GODT. Available at: <http://www.transplant-observatory.org/download/2016-activity-data-report/>. (Accessed: 12th February 2019)
13. Hirsch, H. H. *et al.* Polyomavirus-Associated Nephropathy in Renal Transplantation: Interdisciplinary Analyses and Recommendations. *Transplantation* **79**, 1277–1286 (2005).
14. Drachenberg, C. B. *et al.* Polyomavirus BK Versus JC Replication and Nephropathy in Renal Transplant Recipients: A Prospective Evaluation. *Transplantation* **84**, 323–330 (2007).
15. Chuang, P., Parikh, C. R. & Langone, A. Urinary tract infections after renal transplantation: a retrospective review at two US transplant centers. *Clin. Transplant.* **19**, 230–235 (2005).
16. Burnham, P. *et al.* Single-stranded DNA library preparation uncovers the origin and diversity of ultrashort cell-free DNA in plasma. *Sci. Rep.* **6**, 27859 (2016).
17. Gansauge, M.-T. & Meyer, M. Single-stranded DNA library preparation for the sequencing of ancient or damaged DNA. *Nat. Protoc.* **8**, 737–748 (2013).
18. Bujold, D. *et al.* The International Human Epigenome Consortium Data Portal. *Cell Syst.* **3**, 496–499.e2 (2016).
19. Fernández, J. M. *et al.* The BLUEPRINT Data Analysis Portal. *Cell Syst.* **3**, 491–495.e5 (2016).
20. Albrecht, F., List, M., Bock, C. & Lengauer, T. DeepBlue epigenomic data server: programmatic data retrieval and analysis of epigenome region sets. *Nucleic Acids Res.* **44**, W581–W586 (2016).
21. Bernstein, B. E. *et al.* The NIH Roadmap Epigenomics Mapping Consortium. *Nat. Biotechnol.* **28**, 1045–1048 (2010).
22. ENCODE Project Consortium. The ENCODE (ENCyclopedia Of DNA Elements) Project.

- Science* (80- ). **306**, 636–640 (2004).
23. Jühling, F. *et al.* metilene: fast and sensitive calling of differentially methylated regions from bisulfite sequencing data. *Genome Res.* **26**, 256–62 (2016).
  24. McInnes, L. & Healy, J. UMAP: Uniform Manifold Approximation and Projection for Dimension Reduction. (2018).
  25. Lokk, K. *et al.* DNA methylome profiling of human tissues identifies global and tissue-specific methylation patterns. *Genome Biol.* **15**, 3248 (2014).
  26. Cheng, T. H. T. *et al.* Genomewide bisulfite sequencing reveals the origin and time-dependent fragmentation of urinary cfDNA. *Clin. Biochem.* **50**, 496–501 (2017).
  27. Guo, S. *et al.* Identification of methylation haplotype blocks aids in deconvolution of heterogeneous tissue samples and tumor tissue-of-origin mapping from plasma DNA. *Nat. Genet.* **49**, 635–642 (2017).
  28. Pedersen, B. S., Eyring, K., De, S., Yang, I. V. & Schwartz, D. A. Fast and accurate alignment of long bisulfite-seq reads. (2014).
  29. He, Y. & Ecker, J. R. Non-CG Methylation in the Human Genome. *Annu. Rev. Genomics Hum. Genet.* **16**, 55–77 (2015).
  30. De Vlaminck, I. *et al.* Circulating cell-free DNA enables noninvasive diagnosis of heart transplant rejection. *Sci. Transl. Med.* **6**, 241ra77 (2014).
  31. Beck, J. *et al.* Donor-Derived Cell-Free DNA Is a Novel Universal Biomarker for Allograft Rejection in Solid Organ Transplantation. *Transplant. Proc.* **47**, 2400–2403 (2015).
  32. Lo, Y. M. D. *et al.* Presence of fetal DNA in maternal plasma and serum. *Lancet* **350**, 485–487 (1997).
  33. Koh, W. *et al.* Noninvasive in vivo monitoring of tissue-specific global gene expression in humans. *Proc. Natl. Acad. Sci.* **111**, 7361–7366 (2014).
  34. Mayadas, T. N., Cullere, X. & Lowell, C. A. The multifaceted functions of neutrophils. *Annu. Rev. Pathol.* **9**, 181–218 (2014).
  35. Underhill, H. R. *et al.* Fragment Length of Circulating Tumor DNA. *PLOS Genet.* **12**, e1006162 (2016).
  36. Mouliere, F. *et al.* Enhanced detection of circulating tumor DNA by fragment size analysis. *Sci. Transl. Med.* **10**, eaat4921 (2018).
  37. Tanaka, K. & Okamoto, A. Degradation of DNA by bisulfite treatment. *Bioorg. Med. Chem. Lett.* **17**, 1912–1915 (2007).
  38. Nakazawa, D. *et al.* The responses of macrophages in interaction with neutrophils that undergo NETosis. *J. Autoimmun.* **67**, 19–28 (2016).
  39. Lamers, M. C., de Groot, E. R. & Roos, D. Phagocytosis and degradation of DNA-anti-DNA complexes by human phagocytes I. Assay conditions, quantitative aspects and differences between human blood monocytes and neutrophils. *Eur. J. Immunol.* **11**, 757–764 (1981).
  40. Xia, L. C., Cram, J. A., Chen, T., Fuhrman, J. A. & Sun, F. Accurate Genome Relative Abundance Estimation Based on Shotgun Metagenomic Reads. *PLoS One* **6**, e27992 (2011).
  41. Blauwkamp, T. A. *et al.* Analytical and clinical validation of a microbial cell-free DNA sequencing test for infectious disease. *Nat. Microbiol.* (2019). doi:10.1038/s41564-018-0349-6
  42. Nicolle, L. E. *et al.* Infectious Diseases Society of America Guidelines for the Diagnosis and Treatment of Asymptomatic Bacteriuria in Adults. *Clin. Infect. Dis.* **40**, 643–654 (2005).
  43. Parasuraman, R. & Julian, K. Urinary Tract Infections in Solid Organ Transplantation. *Am. J. Transplant.* **13**, 327–336 (2013).
  44. Snyder, M. W., Kircher, M., Hill, A. J., Daza, R. M. & Shendure, J. Cell-free DNA Comprises an In Vivo Nucleosome Footprint that Informs Its Tissues-Of-Origin. *Cell* **164**, 57–68 (2016).
  45. Song, C.-X. *et al.* 5-Hydroxymethylcytosine signatures in cell-free DNA provide information

- about tumor types and stages. *Cell Res.* **27**, 1231 (2017).
46. Tsalik, E. L. *et al.* Host gene expression classifiers diagnose acute respiratory illness etiology. *Sci. Transl. Med.* **8**, 322ra11 (2016).
  47. Langelier, C. *et al.* Integrating host response and unbiased microbe detection for lower respiratory tract infection diagnosis in critically ill adults. *Proc. Natl. Acad. Sci. U. S. A.* **115**, E12353–E12362 (2018).
  48. Bolger, A. M., Lohse, M. & Usadel, B. Trimmomatic: a flexible trimmer for Illumina sequence data. *Bioinformatics* **30**, 2114–20 (2014).
  49. Li, H. *et al.* The Sequence Alignment/Map format and SAMtools. *Bioinformatics* **25**, 2078–2079 (2009).
  50. Ryan, D. MethylDackel. Available at: <https://github.com/dpryan79/MethylDackel>. (Accessed: 11th March 2018)
  51. Magoč, T. & Salzberg, S. L. FLASH: fast length adjustment of short reads to improve genome assemblies. *Bioinformatics* **27**, 2957–63 (2011).
  52. Altschul, S. F., Gish, W., Miller, W., Myers, E. W. & Lipman, D. J. Basic local alignment search tool. *J. Mol. Biol.* **215**, 403–410 (1990).
  53. Song, Q. *et al.* A Reference Methylome Database and Analysis Pipeline to Facilitate Integrative and Comparative Epigenomics. *PLoS One* **8**, e81148 (2013).
  54. Angermueller, C. *et al.* Parallel single-cell sequencing links transcriptional and epigenetic heterogeneity. *Nat. Methods* **13**, 229–232 (2016).
  55. Ha, G. *et al.* Integrative analysis of genome-wide loss of heterozygosity and monoallelic expression at nucleotide resolution reveals disrupted pathways in triple-negative breast cancer. *Genome Res.* **22**, 1995–2007 (2012).
  56. Zhao, H. *et al.* CrossMap: a versatile tool for coordinate conversion between genome assemblies. *Bioinformatics* **30**, 1006–1007 (2014).
  57. Quinlan, A. R. & Hall, I. M. BEDTools: a flexible suite of utilities for comparing genomic features. *Bioinformatics* **26**, 841–842 (2010).
  58. Houseman, E. A. *et al.* DNA methylation arrays as surrogate measures of cell mixture distribution. *BMC Bioinformatics* **13**, 86 (2012).
  59. Soetaert, K., Van Den Meersche, K. & Van Oevelen, D. *Package limSolve , solving linear inverse models in R.*
  60. Salter, S. J. *et al.* Reagent and laboratory contamination can critically impact sequence-based microbiome analyses. *BMC Biol.* **12**, 87 (2014).

## Supplemental Materials for:

### A cell-free DNA metagenomic sequencing assay that integrates the damage response to infection

**Authors:** Alexandre Pellan Cheng<sup>1</sup>, Philip Burnham<sup>1</sup>, John Richard Lee<sup>2,3</sup>, Matthew Pellan Cheng<sup>4,5</sup>, Manikkam Suthanthiran<sup>2,3</sup>, Darshana Dadhania<sup>2,3,\*</sup>, Iwijn De Vlaminck<sup>1,\*</sup>

\*Correspondence should be addressed to D.D. ([dmd2001@med.cornell.edu](mailto:dmd2001@med.cornell.edu)) or to I.D.V. ([vlaminck@cornell.edu](mailto:vlaminck@cornell.edu)).

\*These authors contributed equally to this work

#### Affiliations:

<sup>1</sup> Meinig School of Biomedical Engineering, Cornell University, Ithaca, NY 14853, USA

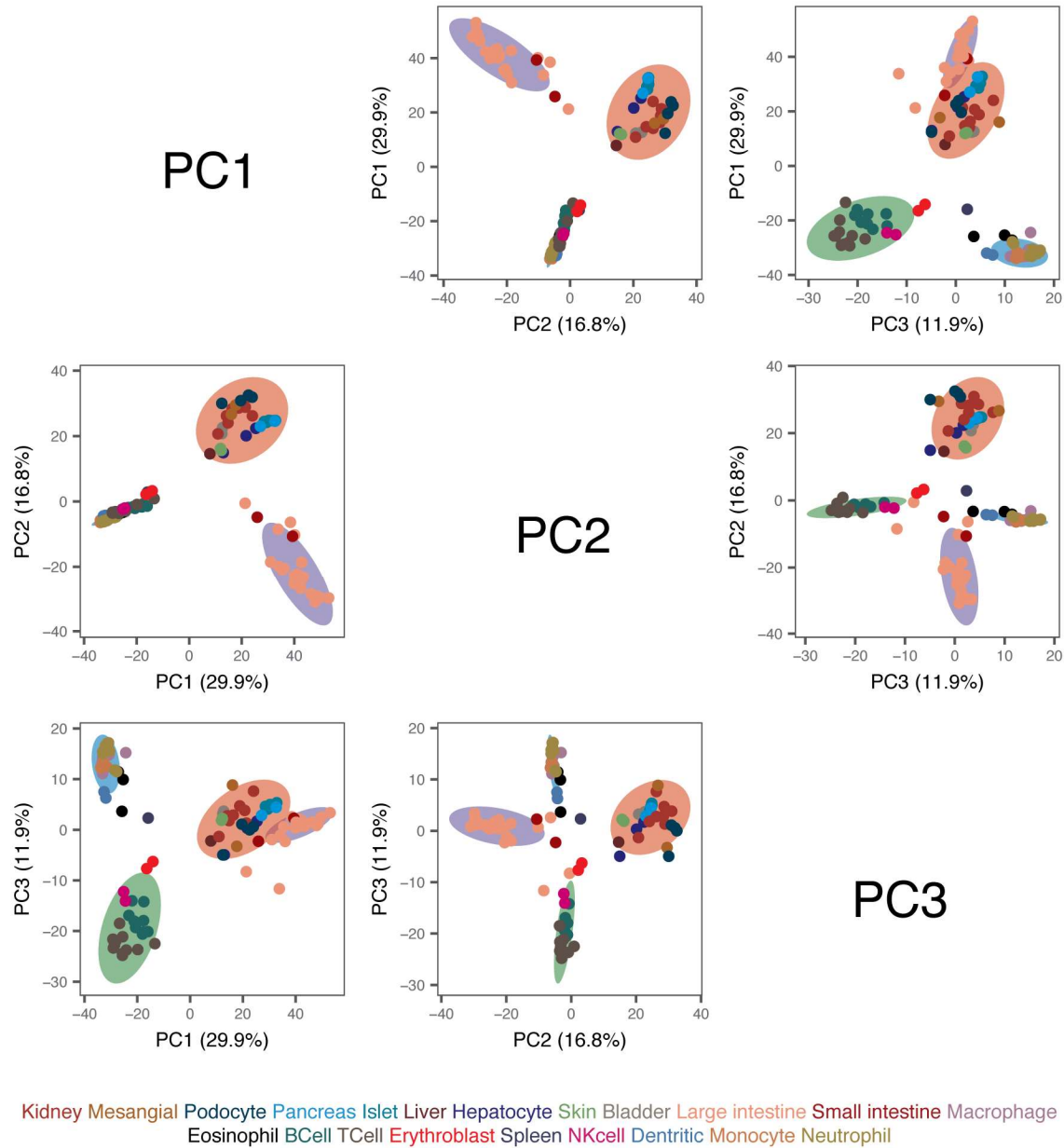
<sup>2</sup> Division of Nephrology and Hypertensions, Department of Medicine, Weill Cornell Medicine, New York, NY 10065, USA

<sup>3</sup> Department of Transplantation Medicine, New York Presbyterian Hospital-Weill Cornell Medical Center, New York, 10065, USA

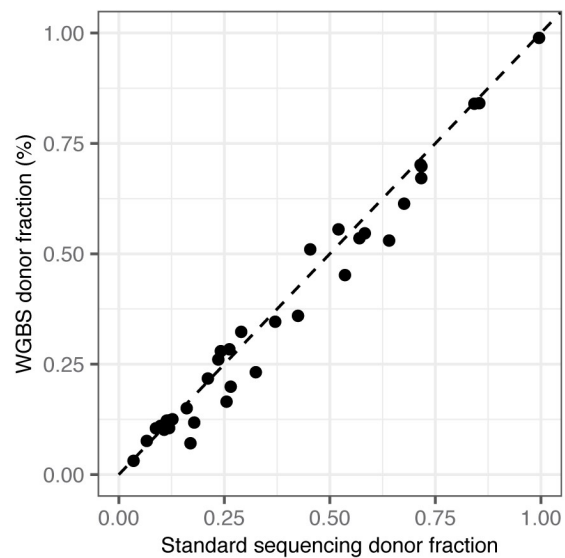
<sup>4</sup> Division of Infectious Diseases, Brigham and Women's Hospital, Boston, Massachusetts

<sup>5</sup> Department of Medical Oncology, Dana-Farber Cancer Institute, Boston, Massachusetts

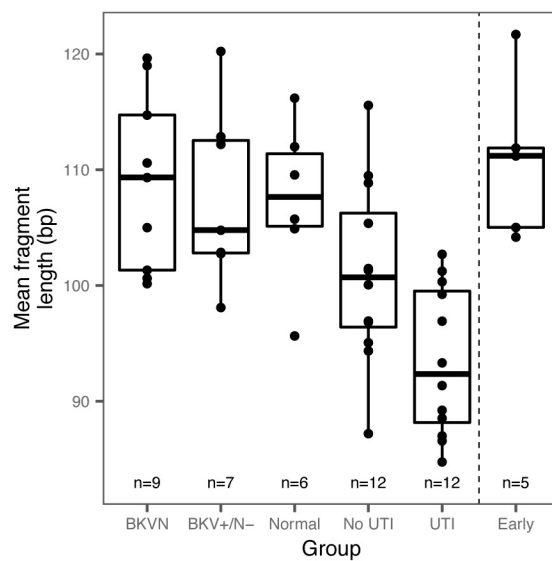




**Supplemental figure 1.** Principal component analysis of reference whole-genome methylation profiles from human tissues.



**Supplementary figure 2.** Comparison of proportion of donor-derived urinary cfDNA measured by conventional and whole-genome bisulfite sequencing (WGBS, n=36 matched samples). Dashed line is a one-to-one slope. Spearman's rho = 0.97, p-value <  $2.2 \times 10^{-16}$ .



**Supplemental figure 3.** Mean fragment length of bisulfite-treated cfDNA for BKVN, BKV+/N-, Normal, no-UTI, UTI and Early groups (n=51).